ACTA MECHANICA SINICA (English Series), Vol.12, No.4, Nov. 1996 ISSN 0567-7718
The Chinese Society of Theoretical and Applied Mechanics
Chinese Journal of Mechanics Press, Beijing, China
Allerton Press, INC., New York, U.S.A.

COMPACT FINITE DIFFERENCE–FOURIER SPECTRAL METHOD FOR THREE–DIMENSIONAL INCOMPRESSIBLE NAVIER–STOKES EQUATIONS*

Xiong Zhongmin (熊忠民) Ling Guocan (凌国灿)
(*LNM, Institute of Mechanics, Chinese Academy of Sciences, Beijing* 100080, *China*)

ABSTRACT: A new compact finite difference–Fourier spectral hybrid method for solving the three dimensional incompressible Navier-Stokes equations is developed in the present paper. The fifth-order upwind compact finite difference schemes for the nonlinear convection terms in the physical space, and the sixth-order center compact schemes for the derivatives in spectral space are described, respectively. The fourth-order compact schemes in a single nine-point cell for solving the Helmholtz equations satisfied by the velocities and pressure in spectral space is derived and its preconditioned conjugate gradient iteration method is studied. The treatment of pressure boundary conditions and the three dimensional non-reflecting outflow boundary conditions are presented. Application to the vortex dislocation evolution in a three dimensional wake is also reported.

KEY WORDS: Compact finite difference, Fourier spectral method, Numerical simulation, Vortex dislocation

1 INTRODUCTION

Direct numerical simulation of the Navier-Stokes equations has become one of the most valuable approaches for the detailed investigation of the flow transition and turbulence phenomena in the past decade. The spectral method[1,2], with relatively fewer independent degrees of freedom and high numerical accuracy, has played an important role in the numerical simulation of turbulence[3~5], especially for those temporally developing flows. However, the requirement of the method on the periodicity of boundary conditions has considerably limited its use in the open space flows such as boundary layers, wakes and jets etc., because this type of flows usually has inflow and outflow boundary conditions and no periodicity can be prescribed in the streamwise direction. The traditional low-order finite difference approximation is usually well suited to this type of boundary conditions, but its numerical accuracy and wave number resolution are too poor to be applicable to the turbulence simulation. Recently, much effort has been devoted to improve the performance of such conventional difference schemes. S.K. Lele[6] proposed the compact finite difference schemes with spectral-like resolution. Fu et al.[7] developed the fifth-order upwind compact schemes. Compared

Received 25 January 1996, revised 5 August 1996
* The project supported by the National Natural Science Foundation of China

with the standard difference schemes, compact schemes can not only achieve higher accuracy on a small computational stencil but also provide much better resolution characteristic, which means it can represent the exact results over a much wider range of wavenumbers on a given mesh. Due to these advantages, compact schemes have begun to be implemented successfully in the compressible flow simulations[7]. However, when they are applied directly to the incompressible flows, some difficulties still exist. Firstly, the direct implementation of finite difference for the incompressible Navier-Stokes equations, though quite flexible in treating the complex boundary conditions, often suffers from the low efficiency, especially when three dimensional iterations are carried out in each step of the time-dependent computations. Secondly, even in the two dimensional case, these kinds of high-order schemes are difficult to be used in their implicit forms, because they can accurately approximate the derivations only in explicit formulations. However, implicit discretizations for velocities and pressure are often necessary in solving the equations to assure the divergence-free constraint and avoid the numerical instability. To overcome these shortcomings, different discretization method (such as spectral, finite difference, finite element) can be introduced in different spatial directions to reduce the total independent degrees of freedom and make the computation more efficient. Furthermore, some kinds of high-order compact schemes that can be used in implicit form are needed to match the high accuracy of the explicit compact approximation. Considering all these points, we propose in this paper a new compact finite difference–Fourier spectral hybrid method to solve the three dimensional incompressible Navier-Stokes equations in primitive variable formulation. The method employs the Fourier spectral discretization in one spatial direction and the high accurate explicit and implicit compact finite difference schemes in the other two directions. The purpose is to provide not only high numerical accuracy and wave number resolution but also the flexible capability in treating the complex boundary conditions. Practical computation for the three dimensional vortex wake evolution proves this hybrid method an effective approach for the numerical simulation of transition in the open space flows.

The paper is organized as follows. First, we discuss the time discretization with the mixed explicit – implicit three-order accuracy scheme and spatial discretization with explicit fifth order upwind compact scheme for convective terms in physical space and the center sixth-order compact schemes for derivatives in spectral space. Then, the implicit compact fourth-order scheme in a nine-point single cell for the Helmholtz equations satisfied by pressure and velocities in spectral space is derived. The efficient preconditioning method of the conjugate gradient iteration is studied. Finally, the proper treatment of pressure boundary conditions and the three dimensional non-reflecting outflow boundary conditions are discussed respectively. As an application, some results of the numerical simulation on the vortex dislocations in a three dimensional wake flow are reported.

2 DESCRIPTION OF COMPACT FINITE DIFFERENCE–FOURIER SPECTRAL METHOD

As a typical configuration for the numerical simulation of three dimensional external flows (e.g., boundary layers, wakes, mixing layers etc.) a hexahedral domain shown in Fig.1 is considered, in which the flow direction and coordinate system are also sketched.

Assuming the periodic boundary condition is adopted in spanwise direction, we expand

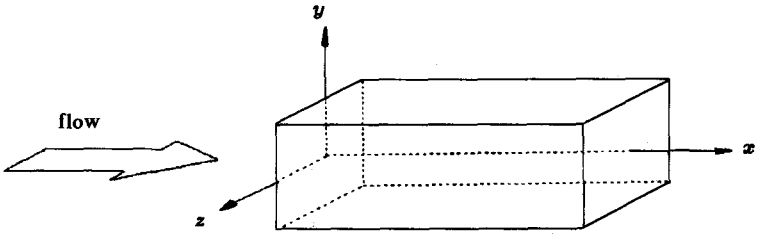

Fig.1 Flow configuration and the coordinate system

all the flow variables as a truncated Fourier series

$$\phi(x,y,z,t)=\sum_{m=-N/2}^{(N/2)-1}\phi_m(x,y,t)\cdot \mathrm{e}^{-\mathrm{i}\cdot m\cdot\beta\cdot Z} \qquad m=-\frac{N}{2},\ \cdots\ ,\ \frac{N}{2}-1 \tag{2.1}$$

where N is the cutoff, β is the spanwise wavenumber. The three dimensional incompressible Navier-Stokes equations in primitive variable formulation are written as

$$\frac{\partial \boldsymbol{u}}{\partial t}+(\boldsymbol{u}\cdot\nabla)\boldsymbol{u}=-\nabla p+\frac{1}{R}\nabla^2\boldsymbol{u} \tag{2.2}$$

where $\boldsymbol{u}=\{u,v,w\}$ are the velocity components in x,y,z directions respectively, p is the pressure and R is the Reynolds number.

Substituting (2.1) into (2.2), and making the inner products on both sides of (2.2) lead to a system of equations for the m^{th} harmonic in a two-dimensional (x,y) domain

$$\frac{\partial \boldsymbol{u}_m}{\partial t}+F_m[(\boldsymbol{u}\cdot\nabla)\boldsymbol{u}]=-\nabla_m p_m+\frac{1}{R}\nabla_m^2\boldsymbol{u}_m \qquad m=-\frac{N}{2},\ \cdots\ ,\ \frac{N}{2}-1 \tag{2.3}$$

where $\nabla_m\equiv\left\{\dfrac{\partial}{\partial x},\dfrac{\partial}{\partial y},-\mathrm{i}m\beta\right\}$, $\nabla_m^2\equiv\left\{\dfrac{\partial^2}{\partial x^2},\dfrac{\partial^2}{\partial y^2},-m^2\beta^2\right\}$, $F_m[(\boldsymbol{u}\cdot\nabla)\boldsymbol{u}]$ is the Fourier transformation of the nonlinear terms. Following the third order mixed explicit-implicit time discretization schemes[8], the solution procedure of Eq.(2.3) can be split into the following three substeps

$$\frac{\boldsymbol{u}'_m-\sum_{q=0}^{J_i-1}\alpha_q\boldsymbol{u}_m^{n-q}}{\Delta t}=-\sum_{q=0}^{J_e-1}\beta_q F_m[(\boldsymbol{u}^{n-q}\cdot\nabla)\boldsymbol{u}^{n-q}] \tag{2.4.1}$$

$$\frac{\boldsymbol{u}''_m-\boldsymbol{u}'_m}{\Delta t}=-\nabla_m p_m^{n+1} \tag{2.4.2}$$

$$\frac{\gamma_0\boldsymbol{u}_m^{n+1}-\boldsymbol{u}''_m}{\Delta t}=\frac{1}{R}\nabla_m^2\boldsymbol{u}_m^{n+1} \tag{2.4.3}$$

where $\boldsymbol{u}'_m,\boldsymbol{u}''_m$ are intermediate velocity fields defined in (2.4.1), (2.4.2). J_i,J_e are parameters for the order of the scheme, $\alpha_q,\beta_q,\gamma_0$ are appropriately chosen weights. For the third order case, the values of these coefficients are summarized as follows[8]:

$$J_e=3,\ J_i=3,\ \alpha_1=3,\ \alpha_2=-\frac{3}{2},\ \alpha_3=\frac{1}{3},\ \beta_1=3,\ \beta_2=-3,\ \beta_3=1,\ \gamma_0=\frac{11}{6}$$

To evaluate the nonlinear term $F_m[(\boldsymbol{u}^{n-q}\cdot\nabla)\boldsymbol{u}^{n-q}]$ in the right hand of (2.4.1), the pseudo-spectral method is adopted. When the Fourier coefficients of velocities are transformed into the velocities in the physical space, the nonlinear convection terms are approximated by the fifth-order upwind compact schemes. According to [7], the form of $u\dfrac{\partial u}{\partial x}$(as an example) can be expressed as

$$\frac{u+|u|}{2}F^+(u)+\frac{u-|u|}{2}F^-(u)$$

where

$$F_i^+ + \frac{2}{3}F_{i-1}^+ = \frac{1}{36}\delta^+\big[-u_{i+1}+11u_i+47u_{i-1}+3u_{i-2}\big]$$

$$F_i^- + \frac{2}{3}F_{i+1}^- = \frac{1}{36}\delta^-\big[-u_{i-1}+11u_i+47u_{i+1}+3u_{i+2}\big]$$

and

$$\delta^{\pm}u_i = \pm(u_{i\pm1}-u_i)/\Delta x$$

$F^+(u), F^-(u)$ are the upwind approximations of first derivations of u for $u>0$ and $u<0$ respectively.

Assuming the boundaries in x direction are labeled by $i=1$ and $i=IN$, then near the boundary $(i=2, IN-1)$, third-order compact schemes are used

$$\frac{2}{3}F_2^+ + \frac{1}{3}F_1^+ = \frac{5}{6}\delta^- u_2 + \frac{1}{6}\delta^+ u_2$$

$$\frac{1}{3}F_{IN}^- + \frac{2}{3}F_{IN-1}^- = \frac{5}{6}\delta^+ u_{IN-1} + \frac{1}{6}\delta^- u_{IN-1}$$

and the second order single side schemes are adopted on the boundary $(i=1, IN)$

$$F_1^+ = (3\delta^+ u_1 - \delta^+ u_2)/2$$

$$F_N^- = (3\delta^- u_N - \delta^- u_{N-1})/2$$

From Eqs.(2.4.2) and (2.4.3), the following kind of Helmholtz equation for the pressure (derived after taking the divergence of (2.4.2)), and velocities must be solved in each step to obtain p_m^{n+1} and $\boldsymbol{u}_m^{n+1}$

$$\frac{\partial^2\varphi}{\partial x^2}+\frac{\partial^2\varphi}{\partial y^2}-b\varphi = f \tag{2.5}$$

The right hand term f includes the derivations of the Fourier coefficients $\boldsymbol{u}_m$ along the x and y directions . They are approximated by the sixth-order center compact schemes which can be expressed as the following form (taking $\dfrac{\partial u_m}{\partial x}$ as an example)

$$\frac{1}{3}F_{i+1}+F_i+\frac{1}{3}F_{i-1} = \frac{14}{9}\delta^0 u_{mi} + \frac{1}{18}\delta^0(u_{m(i+1)}+u_{m(i-1)})$$

where

$$\delta^0 = \frac{1}{2}(\delta^+ + \delta^-)$$

Near the boundary $(i=2, IN-1)$, fourth-order compact schemes are used

$$\frac{1}{6}F_{i+1}+\frac{2}{3}F_i+\frac{1}{6}F_{i-1} = \delta^0 u_{mi}$$

and the second order schemes of single-side are adopted on the boundary ($i = 1, IN$)

$$\frac{2}{3}F_2 + \frac{1}{3}F_1 = \frac{5}{6}\delta^- u_{m2} + \frac{1}{6}\delta^+ u_{m2}$$
$$\frac{1}{3}F_{IN} + \frac{2}{3}F_{IN-1} = \frac{5}{6}\delta^+ u_{m(IN-1)} + \frac{1}{6}\delta^- u_{m(IN-1)}$$

As discussed in the introduction, Eq.(2.5) should be discretized by high order implicit scheme in order to match the high accuracy of the explicit approximation of the $F_m[(\boldsymbol{u}^{n-q} \cdot \nabla)\boldsymbol{u}^{n-q}]$ and f, and meet the numerical stability and convergence requirements. Therefore, the following nine-point compact scheme of fourth-order accuracy is derived

$$\frac{10(\varphi_1+\varphi_3) - 2(\varphi_2+\varphi_4) + (\varphi_5+\varphi_6+\varphi_7+\varphi_8) - 20\phi_0}{(\Delta x)^2} +$$
$$\frac{10(\varphi_2+\varphi_4) - 2(\varphi_1+\varphi_3) + (\varphi_5+\varphi_6+\varphi_7+\varphi_8) - 20\phi_0}{(\Delta y)^2}$$
$$(8\varphi_0 + \varphi_1 + \varphi_2 + \varphi_3 + \varphi_4)b = (8f_0 + f_1 + f_2 + f_3 + f_4)$$

The discretization stencil is shown in Fig.2. The accuracy of this scheme reaches the highest order which can be possibly achieved by a nine-point discretization of Eq.(2.5). Furthermore, the discretization itself results in a standard block tridiagonal coefficient matrix

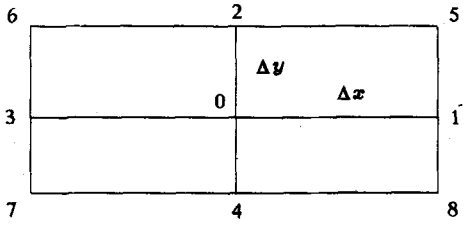

Fig.2 nine-point single cell for the implicit compact scheme

with each block also being tridiagonal. Because these equations must be solved several times at each step, the convergence rate of the corresponding iteration method is crucial to the efficiency of the whole algorithm. The preconditioned conjugate gradient method, due to its rapid convergency, proves to be superior than many other iteration methods. For the preconditioning procedure, though many techniques may be chosen, we find that the pseudo-elimination-k[9] (PE-k) method makes good use of the structure features of this kind matrix and thus greatly accelerates the convergence. Considering the following linear equations

$$\boldsymbol{Q}\boldsymbol{x} = \boldsymbol{b} \tag{2.6}$$

where $\boldsymbol{Q}$ is the block tridiagonal coefficient matrix

$$\boldsymbol{Q} = \begin{Bmatrix} \boldsymbol{B}_1 & \boldsymbol{C}_1 & & & & \\ \boldsymbol{A}_2 & \boldsymbol{B}_2 & \boldsymbol{C}_2 & & & \\ & \ddots & \ddots & \ddots & & \\ & & \ddots & \ddots & \ddots & \\ & & & \boldsymbol{A}_{N-1} & \boldsymbol{B}_{N-1} & \boldsymbol{C}_{N-1} \\ & & & & \boldsymbol{A}_N & \boldsymbol{B}_N \end{Bmatrix}$$

For preconditioning, we can rewrite it as

$$(\boldsymbol{L}^{-1}\boldsymbol{Q}\boldsymbol{U}^{-1})(\boldsymbol{U}\boldsymbol{x}) = \boldsymbol{L}^{-1}\boldsymbol{b} \tag{2.7}$$

Here, $\boldsymbol{L}, \boldsymbol{U}$ are the uncompleted decomposition of $\boldsymbol{Q}$, and can be expressed as

$$\boldsymbol{L} = \begin{Bmatrix} \boldsymbol{S}_1 & & & & & \\ \boldsymbol{A}_2 & \boldsymbol{S}_2 & & & & \\ \ddots & \ddots & & & & \\ & \ddots & \ddots & & & \\ & & \boldsymbol{A}_{N-1} & \boldsymbol{S}_{N-1} & & \\ & & & \boldsymbol{A}_N & \boldsymbol{S}_N \end{Bmatrix}$$

$$\boldsymbol{U} = \begin{Bmatrix} \boldsymbol{I}_1 & \boldsymbol{T}_1 & & & & \\ & \boldsymbol{I}_2 & \boldsymbol{T}_2 & & & \\ & \ddots & \ddots & & & \\ & & \ddots & \ddots & & \\ & & & \boldsymbol{I}_{N-1} & \boldsymbol{T}_{N-1} & \\ & & & & \boldsymbol{I}_N & \end{Bmatrix}$$

where, S, T are given by

$$\begin{aligned} &\boldsymbol{S}_1 = \boldsymbol{B}_1 \\ &\boldsymbol{T}_i = \boldsymbol{S}_i^{-1}\boldsymbol{C}_i \qquad\qquad i = 1, 2, \cdots, N-1 \\ &\boldsymbol{S}_i = \boldsymbol{B}_i(\boldsymbol{I}_i + k\boldsymbol{B}_i^{-1}\boldsymbol{A}_i\boldsymbol{B}_{i-1}^{-1}\boldsymbol{C}_{i-1})^{-1} \end{aligned}$$

I_i is the identity matrix, k is the optimization coefficient for speeding up the convergence. Since the classical conjugate gradient method requires the coefficient matrix to be symmetry and positive definite, we apply it to the normal equation of (2.7) and the solution can be found quickly. For example, considering the following model equation

$$\frac{\partial^2\varphi}{\partial x^2} + \frac{\partial^2\varphi}{\partial y^2} - \varphi = -3\sin x\cos y \qquad (x, y) \in [0, 2\pi] \times [0, 2\pi]$$

with all Dirichlet boundary conditions, Table 1 gives a comparison on the performance of the PE-k and SOR with Chebyshev acceleration under different grid sizes.

Table 1 Comparison of iteration numbers and time of SOR-C and PE-k

Grid	$N_{\text{SOR-C}}$	$N_{\text{PE-k}}$	$T_{\text{PE-k}}/T_{\text{SOR-C}}$	k
41 × 41	108	3	20%	2.7
61 × 61	167	4	14%	3.0
81 × 81	227	4	12%	3.3
101 × 101	286	3	8%	3.4

Note: SOR-C: SOR with Chebyshev acceleration; N: Iteration numbers; T: Computer time.

It is clearly shown that the computational efficiency by PE-k method is usually an order of magnitude higher than that of SOR with Chebyshev acceleration.

With regard to the numerical simulation of the open space flows, the correct treatment of the boundary conditions is very important because it not only affects directly the overall accuracy of the scheme, but also determines the efficiency of the time-stepping algorithm. This is especially true for the pressure boundary conditions and the outflow boundary conditions. From Eq.(2.3) and (2.4), the semi-discretized pressure boundary conditions can be expressed as

$$\frac{\partial p_m^{n+1}}{\partial n} = \boldsymbol{n}\cdot\Big\{-\frac{\partial \boldsymbol{u}_m}{\partial t}+\frac{1}{R}\nabla^2\boldsymbol{u}_m^{n+1}-\sum_{q=0}^{J_c-1}\beta_q F_m\big[(\boldsymbol{u}^{n-q}\cdot\nabla)\boldsymbol{u}^{n-q}\big]\Big\}=$$

$$\boldsymbol{n}\cdot\Big\{-\frac{\partial \boldsymbol{u}_m}{\partial t}-\frac{1}{R}F_m[\nabla\times\Omega^n]-\sum_{q=0}^{J_c-1}\beta_q F_m\big[(\boldsymbol{u}^{n-q}\cdot\nabla)\boldsymbol{u}^{n-q}\big]\Big\}$$

where $\nabla^2\boldsymbol{u}\equiv\nabla D-\nabla\times\Omega$, $\Omega\equiv\nabla\times\boldsymbol{u}$, $D\equiv\nabla\cdot\boldsymbol{u}$ is used. By forcing $D^{n+1}\equiv 0$, in each time step and replacing $\nabla\times\Omega^{n+1}$ by $\nabla\times\Omega^n$, the divergence-free constraint can be well satisfied on the boundaries. In addition, for the pressure Fourier coefficient p_0, Equation (2.5) becomes a Poisson equation with all Neumann boundary conditions, the coefficient matrix Q is therefore singular. The solvable condition must be employed to remove the singularity of Q before preconditioned conjugate gradient method can be applied.

The study of the outflow boundary conditions in the incompressible flow, generally speaking, is quite insufficient. It is hoped that the outflow boundary conditions can closely approximate the free space situation which exists in the absence of these boundaries. Otherwise, the spurious perturbation waves may propagate upstream and severely affect the accuracy of computation in the inner flow domain. Recently, G. Jin et al.[10] developed a new kind of nonreflecting-type outflow boundary conditions on the analogy of the classical wave equation. It deals with both the nonlinear and diffusive mechanisms of flow and well matches the Navier-Stoke equations adopted inside the domain. By preliminary computations, we find the performance of this kind of boundary condition is quite suitable to the numerical simulation of external flows, especially those involving the interaction between waves and vortices. Generalized to the three dimensional case, the nonreflecting boundary condition in physical space can be formulated as

$$\frac{\partial \boldsymbol{u}}{\partial t}+u\frac{\partial \boldsymbol{u}}{\partial x}=\frac{1}{R}\Big(\frac{\partial^2\boldsymbol{u}}{\partial y^2}+\frac{\partial^2\boldsymbol{u}}{\partial z^2}\Big) \tag{2.8}$$

We noticed that the similar result was also obtained in [11] recently. The corresponding spectral form used in the computation is

$$\frac{\partial \boldsymbol{u}_m}{\partial t}+F_m\Big[u\frac{\partial \boldsymbol{u}}{\partial x}\Big]=\frac{1}{R}\Big(\frac{\partial^2\boldsymbol{u}_m}{\partial y^2}-m^2\beta^2\boldsymbol{u}_m\Big) \tag{2.9}$$

These Eqs.(2.9) must be solved simultaneously with the same third order mixed explicit-implicit schemes adopted for the inner Navier-Stokes equations.

3 APPLICATION TO 3-D VORTEX WAKE

As a typical kind of open space flow—three dimensional wake behind a cylinder has been the focus of many recent studies in order to understand its complex transition mechanism. It is found that during the transition from the 2-D laminar Karman vortices to 3-D

turbulence, vortex dislocation[12] is one of the fundamental physical phenomena. Unlike the ordinary occurrence of three dimensional transition which takes the form of spanwise unstable waves and second instability mechanism, vortex dislocations are mainly induced by local disturbances or defects. Typically, they are initiated by the phase variations between the spanwise vortex cells with different shedding frequencies during the processes of vortex formation. While moving downstream, these dislocations grow into large-scale structures and bring about a series of complex distortions on the laminar Karman vortices and finally make them breakdown into turbulence. Moreover, there are a number of other different types of flows exhibiting similar features of the vortex dislocation during their transitions, such as spatially growing free shear layer[13,14], flows past a non-uniform body geometry[15] and even the Reyleigh-Benard convection patterns[16]. It is believed that there is a new kind of transition mechanism associated with the vortex dislocation and many recent studies have been undertaken to investigate its dynamics. However, the basic understanding of the vortex dislocations is, until now, mainly from experimental studies, and the numerical study, though important to the understanding of the mechanism, has not been reported as to the knowledge of the authors. This is partly because some difficulties must be overcome before this three dimensional time dependent computation can be performed, such as the large space domain (corresponding to the streamwise characteristic scale of the vortex dislocation which is usually much lager than the wavelength of the basic Karman vortex street), the wavenumber resolution and accuracy of the numerical method, treatment of the inflow and outflow boundary conditions as well as the efficiency of the computation. As an application of the compact finite difference–Fourier spectral method described above, the numerical simulation for the evolution of vortex dislocations in the three dimensional wake was carried out. The fundamental characteristics such as the vortex tearing and reconnection, the axial velocity generation and the spanwise "climbing"[12], are successfully reproduced. It is felt that these results will be of much help in understanding the transition physics of vortex dislocation in the open space flows.

Normalized by the diameter of the cylinder and the oncoming potential velocity, the computational domain is 60, 30, 30 on streamwise, vertical and spanwise directions, respectively. The cutoff of the truncated Fourier series is $N = 32$, and the corresponding number of the grid points in x-y plane is 122×62. The inflow velocity profile is taken as

$$U(y,z) = 1.0 - a(z) \cdot (2.0 - \cosh(by)^2)\mathrm{e}^{-(cy)^2} \tag{3.1}$$

where $a = 1.1 + 0.4e^{-z^2}, b = 1.1, c = 1.2$, which are determined according to the mean velocity profile in the near cylinder wake obtained from the direct numerical simulations[17] as well as the experimental measurements[18]. The distribution along y of $U(y,z)$ is absolutely unstable, and the variation along z represents a local three dimensional disturbance on a 2-D cylinder. The Reynolds number is taken as 200. The iso-vorticity surface is shown in Fig.3, and the colours on the vortex rolls represent the different values of the spanwise velocity. As expected from the theoretical instability analysis based on the 2-D velocity profiles along y, the two dimensional vortex street is developed by the intrinsic global instability at the spanwise locations far from $z = 0$ in Fig.3. The wavelength of the 2-D rollers is around five times of the cylinder diameter, which is in agreement with the many experimental results. In the middle regions near $z = 0$, a symmetry dislocation occurs due to the different shedding frequencies associated with the spanwise variation of the velocity profiles. The

distortion and tearing[19] of the spanwise vortices, the formation of the streamwise vortices and their connection with spanwise vortices, are shown by the iso-vorticity surface. These calculated structures are compared well with the typical topological changes of the vortices during dislocations observed by flow visualization in experiments[12~14]. Another important

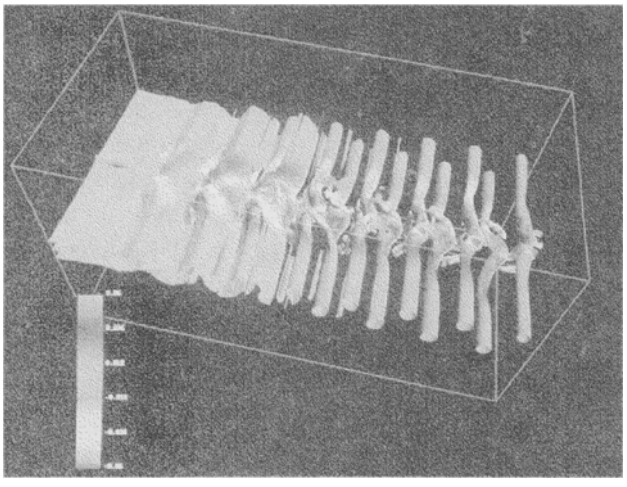

Fig.3 The iso-vorticity surface in a 3D wake with vortex dislocations and the spatial distribution of spanwise velocity

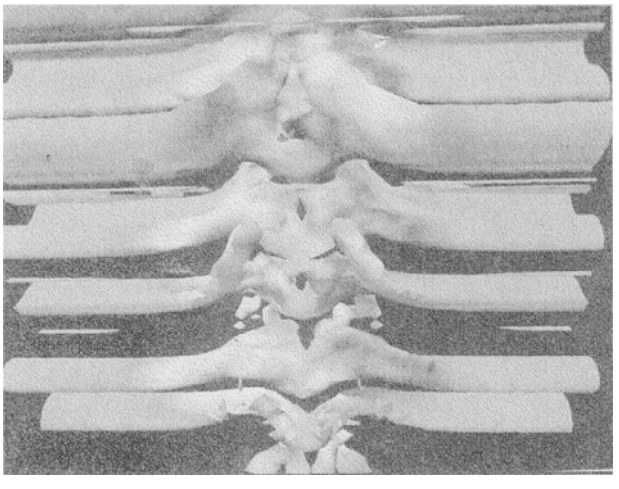

Fig.4 A close-up of the vortex splitting during the formation of vortex dislocations

feature of the vortex dislocation — spanwise "climbing" — has also been reproduced. Fig.4 is a top view showing a close-up of the vortex splitting process during the formation of the dislocation. The flow is downwards and the spanwise velocity is represented by the colours whose legend is the same as Fig.3. It can be clearly seen that the spanwise velocities are generated form the complex vortex tearing and lead in turn to a rapid lateral spreading from the dislocation center. Fig.5 gives a concept model of the vortex splitting and reconnection in the dislocations. Owing to the limitation of space, a full analysis and discussion on the simulation results of the vortex dislocations will be published elsewhere.

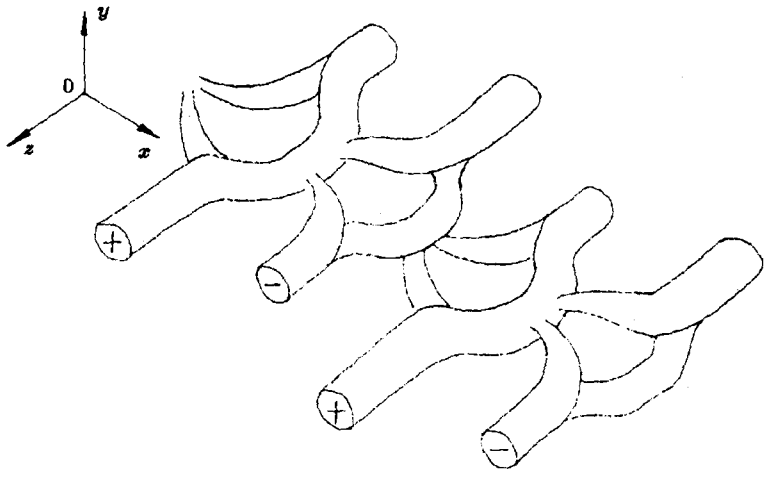

Fig.5 A concept model for the vortex splitting and reconnection in the dislocations

4 CONCLUDING REMARKS

In the present paper, we present a new hybrid numerical method for solving three dimensional incompressible Navier-Stokes equations which takes the advantages of both the Fourier spectral expansion and compact finite difference approximation. The high order upwind and center compact finite difference schemes are described respectively. The preconditioned conjugate gradient iteration method for solving the Helmholtz equation discretized by nine-point implicit compact scheme in spectral space is studied in detail and proves to be quite efficient. The flexibility of the algorithm for the complex boundary conditions makes it especially useful in the numerical simulation of the open space flows. Application to the vortex dislocation evolution in a three dimensional wake is discussed. Combined with the domain decomposition approach, this method may be used in the more complex flow configurations. The three dimensional nonreflecting outflow boundary conditions presented in this paper will also be useful in the numerical simulation of other open space flows such as boundary layers, jets, mixing layers etc.

Acknowledgement The first author is grateful to Prof. Fu Dexun and Prof. Ma Yanwen for introducing him to the upwind compact difference schemes and many useful discussions. The authors are also thankful to Dr. X. Fang for the assistance in the data visualization and colour picture presentations on the Silicon Graphics workstation.

REFERENCES

1 Gottlieb D,Orszag SA. Numerical Analysis of Spectral Methods: Theory and application. (SIAM-CBMS, Philadelphia), 1977

2 Canuto C, Hussaini MY, Quarteroni A, Zang TA. Spectral Methods in Fluid Dynamics. New York, Springer-Verlag, 1988

3 Rogallo R, Moin P. Numerical simulation of turbulent flows. *Annu Rev Fluid Mech*, 1984, 16: 99~137

4 Kim J, Moin P, Moser RD. Turbulent statistics in a fully-developed channel flow at low Reynolds

number. *J Fluid Mech*, 1987, 177: 133~166

5 Spalart P. Direct simulation of a turbulent boundary layer up to $Re_\theta = 1410$. *J Fluid Mech*, 1988, 187: 61~98

6 Lele SK. Compact finite difference schemes with spectral-like resolution. *J Comput Phys*, 1992, 103: 16~42

7 Fu Dexun, Ma Yanwen. Numerical simulation of coherent structures in mixing layer. *Science in China*, 1996, 26(A7): 657~664 (in Chinese)

8 Karniadakis GE, Israeli M, Orzag SA. High-order splitting methods for the incompressible Navier-Stokes equations. *J Comput Phys*, 1991, 97: 414~443

9 Hu Jiagan. Iteration Methods for the Linear Algebra Equations. Beijing: Science Press, 1991 (in Chinese)

10 Jin G, Braza M. A nonreflecting outlet boundary condition for incompressible unsteady Navier-Stokes calculation. *J Comput Phys*, 1993, 107: 239~253

11 Persillon H, Braza M, Jin G. Prediction of Transition features in the flow past a circular cylinder in three-dimension. Proceedings of the Fifth International Offshore and Polar Engineering Conference, the Hague, the Netherlands, June 11–16, 1995. 597~602

12 Williamson CHK. The natural and forced formation of spot-like 'vortex dislocations' in the transition of a wake. *J Fluid Mech*, 1992, 243: 393~441

13 Browand FK, Legendre S, Taniguchi P. A model of vortex pairing induced by defects in mixing layer. *Bull Am Phys Soc*, 1989, 34:2269

14 Nygarrd KJ, Glezer A. Core instability of the spanwise vortices in a plane mixing layer. *Phys Fluids*, 1990, A2:461~464

15 Lewis C, Gharib M. An exploration of the wake three-dimensionalities caused by a local discontinuity in cylinder diameter. *Phys Fluids*, 1992, A4: 104~117

16 Pocheau A, Croquette V, Le Gal P. Turbulence in a cylinderical container of Argon near threshold of convection. *Phys Rev Lett*, 1985, 55:1094~1097

17 Triantafyllou G S, Karniadakis GE. Computational reducibility of unsteady viscous flows. *Phys Fluids*, 1990, A2:653~656

18 Nishioka M, Sato H. Measurements of velocity distributions in the wake of a circular cylinder at low Reynolds numbers. *J Fluid Mech*, 1974, 65: 97~122

19 Eisenlohr H, Eekelmann H. Vortex splitting and its consequences in the vortex street wake of cylinders at low Reynolds number. *Phys Fluids*, 1989, A1: 189~192